Rapid visualization of chemically related compounds using Kendrick mass defect as a filter in mass spectrometry imaging

Kune Christopher[a]‡ and Mc Cann Andréa[a]‡, La Rocca Raphaël[a], Arguelles Arias Anthony[b], Tiquet Mathieu[a], Van Kruining Daan[c], Martinez Martinez Pilar[c], Ongena Marc[b], Eppe Gauthier[a], Quinton Loïc[a], Far Johann[a], De Pauw Edwin[a*]

[a]Mass Spectrometry Laboratory, MolSys Research Unit, University of Liège, Liège, Belgium,

[b]Microbial Processes and Interactions, Gembloux Agro-Bio Tech, TERRA Teaching and Research Centre, University of Liege, Gembloux, Belgium.

[c] Department of Psychiatry and Neuropsychology, School for Mental Health and Neuroscience, Maastricht University, Maastricht, the Netherlands.

ABSTRACT: Kendrick mass defect (KMD) analysis is widely used for helping the detection and identification of chemically related compounds based on exact mass measurements. We report here the use of KMD as a criterion for filtering complex mass spectrometry data. The method enables an automated, faster and efficient data processing, enabling the reconstruction of 2D distributions of family of homologous compound in MSI images. We show that the KMD filtering, based on a homemade software, is suitable for low resolution (full width at half-maximum, FWHM, at *m/z* 410 of 20 000) and high resolution (FWHM, at *m/z* 410 of 160 000) MSI data. This method has been successfully applied to two different types of samples, bacteria co-cultures and brain tissue section.

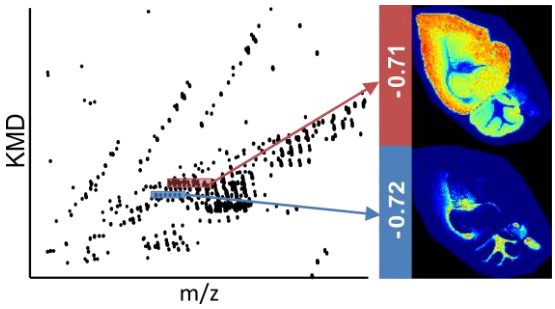

Identification of analytes in complex mixtures is still a major challenge in analytical chemistry[1]. For that purpose, mass spectrometers are among the most widely used instruments. They are commonly coupled to direct infusion or hyphenated with separation techniques, e.g., liquid chromatography (LC), capillary electrophoresis (CE), ion mobility spectrometry (IMS). Mass spectrometry imaging (MSI) is a particular case in which 2D distribution of analytes can be reconstructed after recording full mass spectra at the coordinate of the "pixels" sampled by a LASER beam. The resolution power and the accuracy of analyzers greatly improved to reach values allowing the direct determination of molecular formula of low mass range analytes. However the extraction of chemical information from spectra is now a bottleneck due to the massive amount of information contained in HR MS data[2].

Kendrick[3] introduced in 1963 a method based on two-dimensional projection of the atomic composition space allowing a rapid identification of families of molecules. The Kendrick method is based on the transformation of the mass spectra (mass-to charge ratio or *m/z* in the X-axis and intensity in the Y-axis) to Kendrick plots where the X-axis corresponds to the Kendrick mass (KM) and the Y-axis corresponds to the Kendrick mass defect (KMD). The KM is defined by converting the exact masses of a given group of atoms (the Kendrick base) to the nearest integer value in atomic mass unit (amu). Kendrick method changes the IUPAC amu reference (i.e. 1/12 of the ^{12}C mass) to another mass unit (e.g. 1/14 of the $^{12}C^{1}H_2$ radical mass). KM can be calculated from *m/z* value by the Equation 1 where the Nominal-$M_{Kendrick\ reference}$ and $M_{Kendrick\ reference}$ are respectively the nominal mass and the exact mass of the Kendrick reference used for the atomic mass unit definition.

$$KM = m/z \times \frac{Nominal - M_{Kendrick\ Reference}}{M_{Kendrick\ Reference}} \quad (1)$$

The KMD corresponds to the difference between the rounded KM values and the KM (Eq. 2).

$$KMD = round(KM) - KM \quad (2)$$

All the compounds differing only by the number of repeating unit of the Kendrick reference will have the same KMD for different KM. Consequently, chemically related compounds will be aligned in the KMD axis on the Kendrick plot, making their identification easier. Recently higher order Kendrick transformations have also been applied when oblique correlations suggest the presence of a further repeating unit[4]. Over the years, KMD analysis has been extended to the analysis of complex samples composed of chemically related structures, such as petrochemicals, but also polymers or lipids[5-11].

In this paper, we show that the KMD, which is specific to chemically related homologous series of compounds, can be

used to replace the *m/z* axis of the mean spectra classically used for the analysis of images in MSI. The KMD can be adjusted to filter data in a non-targeted, semi-targeted and targeted mode. This approach enables an automated, faster and efficient data processing, allowing the rapid identification and localization of families of compounds in the complex chemical space of the image. This method has been successfully applied to two different types of samples, bacteria co-cultures and brain tissue sections.

MATERIALS AND METHODS

Materials. The MALDI matrices 2,3-Diaminonaphthalene (DAN) and α-Cyano-4-hydroxycinnamic acid (HCCA) were purchased from Sigma-Aldrich (Belgium). Acetonitrile and Methanol were LC-MS grade from Sigma-Aldrich (Belgium). Poly(ethylene oxide) monomethylether (CH3O-PEO-H) having an average nominal mass of 750 g/mol, tetraalkylammonium bromides (reagent grade >98%), bovine serum albumin (BSA), and sodium chloride were purchased from Sigma-Aldrich (Belgium). Pr. Philippe Jacques (Terra Teaching and Research Center, Microbial Processes and Interactions, University of Liège, Belgium) and Lipofabrik (Lille, France) kindly provided standards of lipopeptides.

Sample preparation for MALDI-FT-ICR MS imaging proof of concept. DAN matrix solution was prepared at saturation (>30mg/mL) in ACN/water 70:30 vol/vol spiked with 0.2% TFA. Tetraalkylammonium bromide stock solution was dissolved in ACN to reach the final concentration of 10µM. Trypsin digestion of BSA using MS grade porcine trypsin (purchased from PIERCE, Thermofisher, Belgium) was prepared at a final concentration of 15 µM in 50% methanol spiked with 0.1% formic acid following the procedure described in supporting information. Lipids were extracted from cultured eukaryotic cells based on Matysah protocol [12] and resuspended in MeOH. Lipopeptides were dissolved in MeOH spiked with 0.1% TFA at final concentration of 10µM. CH_3O-PEO-H was dissolved in ACN 10µM NaCl to reach a concentration of 10µM. Each sample was mixed separately with DAN matrix at a ratio of 1:1, and were spotted randomly on a MALDI AnchorChip target plate (Bruker, Bremen, Germany) in duplicate for high and low resolution MS imaging. In addition, 1µL of each sample was mixed and DAN matrix was added at a 1:1 ratio and spotted onto the MALDI target plate. Finally, a spot of DAN matrix was added.

Bacterial Strains, medium and Culture conditions. The strains used for this study were *Bacillus velezensis GA1* and *Pseudomonas sp. CMR12a*. Both strains were inoculated on a semi-solid agar-based PDA medium (Potato Dextrose Agar) and incubated overnight at 30°C. At the end of the culture, petri dishes were sealed with Parafilm M ® and stored at 4°C prior to analysis.

Animals, tissue sampling and sectioning. Mouse brain samples were provided by Prof. Martinez (School of Mental Health and Neuroscience at Maastricht University the Netherlands), and bred in house as described elsewhere[13]. Animals were sacrificed by CO_2 inhalation and brain tissues were extracted. After extraction, the brains were cut across the sagittal midline and immediately fresh-frozen in liquid nitrogen. The brain parts were subsequently stored at -80 °C. On the day of transport, samples were placed on dry ice and transferred to the University of Liege. All procedures were approved by the Animal Welfare Committee of Maastricht University and were performed according to Dutch federal regulations for animal protection. Frozen brain tissues were sectioned into 14-µm thick sagittal slices using a CryoStar NX70 (Thermo Fisher Scientific, Massachusetts, USA) at -20°C and thaw-mounted onto indium-tin oxide (ITO) conductive glass slides (Bruker Daltonics, Bremen, Germany).

Sample preparation for MALDI-FT-ICR MS imaging. Microbial colonies on agar and region of interest were cut directly from the petri dish and transferred to the target ITO plate (Bruker, Bremen, Germany), previously covered with double sided conductive carbon tape (StructureProbe INC, West Chester, PA, USA). This assembly was then placed in a vacuum desiccator until complete drying (overnight). An HCCA matrix solution was prepared at the concentration of 5mg/mL in ACN/water 70:30 vol/vol spiked with 0.2% TFA, based on the previous work of Debois et al[14]. Application of the matrix solution on the dried bacterial sample was performed using the SunCollect (SunChrom, Friedrichsdorf, Germany) spraying system. In total, 60 layers of HCCA matrix were sprayed on the sample. The three first layers were sprayed at 5µL/min, and the other at 10µL/min. Mouse brain tissue slides deposed on ITO slides were first put into a vacuum desiccator for approximatively 20 minutes. A solution of HCCA at the concentration of 5mg/mL in MeOH/water 90:10 vol/vol spiked with 0.2% TFA was prepared, and sprayed onto the dried sample by the SunCollect. The number of spraying layers were set to 30, at a spraying speed of 10µL/min, excepted for the three first layers sprayed at 5µL/min.

FT-ICR Mass spectrometry. Mass spectrometry images were obtained using a FT-ICR mass spectrometer (SolariX XR 9.4T, Bruker Daltonics, Bremen, Germany). The mass spectrometer was systematically mass calibrated from 200 *m/z* to 2,300 *m/z* before each analysis with a red phosphorous solution in acetone spotted directly onto the ITO Glass slide or onto the MALDI plate to reach a mass accuracy better than 0.5ppm PPM. FlexImaging 5.0 (Bruker Daltonics, Bremen, Germany) software was used for MALDI MS imaging acquisition, with a pixel step size for the surface raster set to 150µm for Kendrick proof of concept imaging and to 100µm for bacteria and brain tissue imaging. For each mass spectrum, one scan of 20 LASER shots was performed at a repetition of rate 200Hz. The LASER power was set to 50% and the beam focus was set to "small". The mass spectra for high and low resolution images were recorded by setting the number of datapoints in the transient at respectively 1 000 000 and 256 000.

Kendrick filtering for data reduction and clustering. MSconvert (Proteowizard)[15] and Fleximaging 5.0 (Bruker) have been used to, respectively, convert MS raw files to mzML and MSI raw files to imzML files. These files are then processed in our Python homemade software allowing data filtering based on KMD. The Kendrick filtering method workflow is reported in Figure 1. The first step consists in the extraction of mass spectra for each pixel and noise reduction of the MS spectra based on an intensity threshold (100,000 counts per scan for this work). All extracted mass spectra are normalized to the total ion count (TIC). The software calculates for each *m/z* value a Kendrick mass defect (KMD) value using Eq. 1 and Eq. 2 in the user-defined Kendrick reference (-CH_2- for this work). Different rounding functions are available in this software, i.e. floor, ceil, and round (floor is used for the reported results). All *m/z* ratio are then associated to a KMD (comprised between 0 and -1). The second step aims to reduce the MS data by conserving only ions for which KMD values are similar. The selected KMD values can be entered by the user with a defined tolerance. An *m/z* ratio selection range can also be applied as a criterion for the data filtering. The software allows a user-

defined *m/z* tolerance value (5 ppm and 1 ppm for mass spectra with resolution of, respectively, 20,000 and 160,000 full width at half-maximum, FWHM, at 410 *m/z*). The resulting reduced mass spectra corresponds to the chemically related compounds. In the case of different compound families sharing a similar KMD, an additional algorithm is added to cluster the conserved ion by compound families. This clustering step (reported as mass difference clustering algorithm in Figure 1) groups ions for which the mass difference corresponds to a multiple of the chosen Kendrick reference mass. Different mass lists are then generated for each detected compound family. Finally, one image is generated for each mass list obtained after data reduction by the KMD filtering and the mass difference clustering algorithm. All this process can be repeated with different KMD and *m/z* ranges to generate additional MS images of different compound families. Moreover, the software is able to clean the spectra by removing one or several *m/z* values from a mass list before to reconstruct the image.

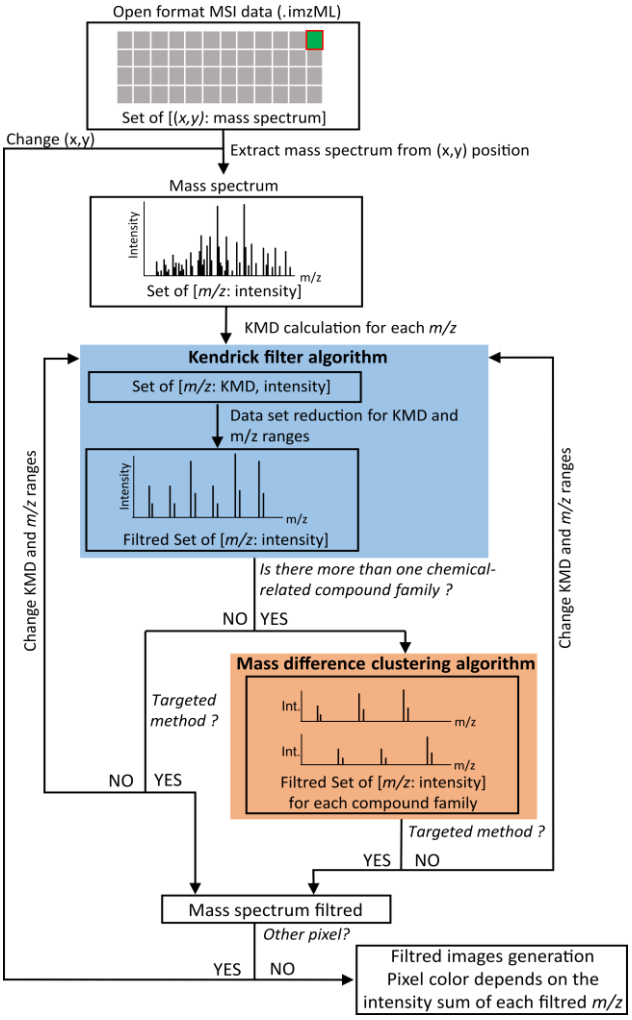

Figure 1: Kendrick filtering method workflow applied on MSI data

RESULTS AND DISCUSSIONS

KMD filtering concept. The illustration of the KMD filtering concept is shown in Figure 2 for a MALDI FT-ICR MS data. The MALDI spot was containing a mix of different compound families such as lipids, lipopeptides, polymers, tetraalkylammonium and peptides of BSA tryptic digest. The resulting mass spectra (Figure 2.B) is complex and the attribution of MS peak to the compounds family is challenging. However, the Kendrick plot (Figure 2.A) generated using $-CH_2-$ as Kendrick reference allows the alignment of compound with repeating unit of $-CH_2-$. Tetraalkylammonium, lipids and lipopeptides families are then easily detected (respectively highlighted in blue, green and orange). Polymers families can also be observed by changing the Kendrick reference to the repeated monomer unit in theses polymers (See Supporting information Figure S2). The aim of the proposed Kendrick filtering method is to extract only from the mass spectra the peaks corresponding to a given family of compounds and to generate a new filtered spectrum, chromatogram, mobilogram or image. Depending on the mass spectrometer resolution, setting a KMD range as well as an MS range might not be enough to isolate a single family of chemically related compounds. This can be explained by the presence of other compounds having similar KMD and *m/z*. In these cases, the mass difference filtering algorithm (see materials and methods section) can be used to separate overlapping families of compounds. By applying the KMD filtering followed by the mass difference clustering, clean filtered spectra are obtained for each different family in the MALDI spot such as tetraalkylammonium (Figure 2.C), the surfactins (lipopeptides family, Figure 2.D) and the phosphatidylcholines (lipid family, Figure 2.E).

KMD filtering concept. To verify the application of KMD filtering on MSI data, we generated a proof of concept by imaging a MALDI AnchorChip target plate where lipids, Tetraalkylammonium salts, lipopeptpides and polymers were randomly spotted (Figure 3.A). The presented KMD filtering algorithm was applied on the imaging data. The MSI data were acquired with two different MS resolution calculated at the *m/z* 410 (i.e. 20,000 and 160,000). A mixture spot (spot 8, containing all the investigated compound families) and an empty spot (Spot 3, containing only the matrix) have been added as, respectively, a positive and a negative control. As expected, none of the targeted compounds were found in the negative control spot. The KMD filtering allowed the determination of the localization of each chemically related compounds independently of the MS resolution. The detection of these compounds was possible no matter the sample complexity, confirming the power of KMD filtering. This result suggests that the KMD filtering could be applied to MSI data generated from MS analyzer with different MS resolutions (TOF, Orbitrap, FT-ICR).

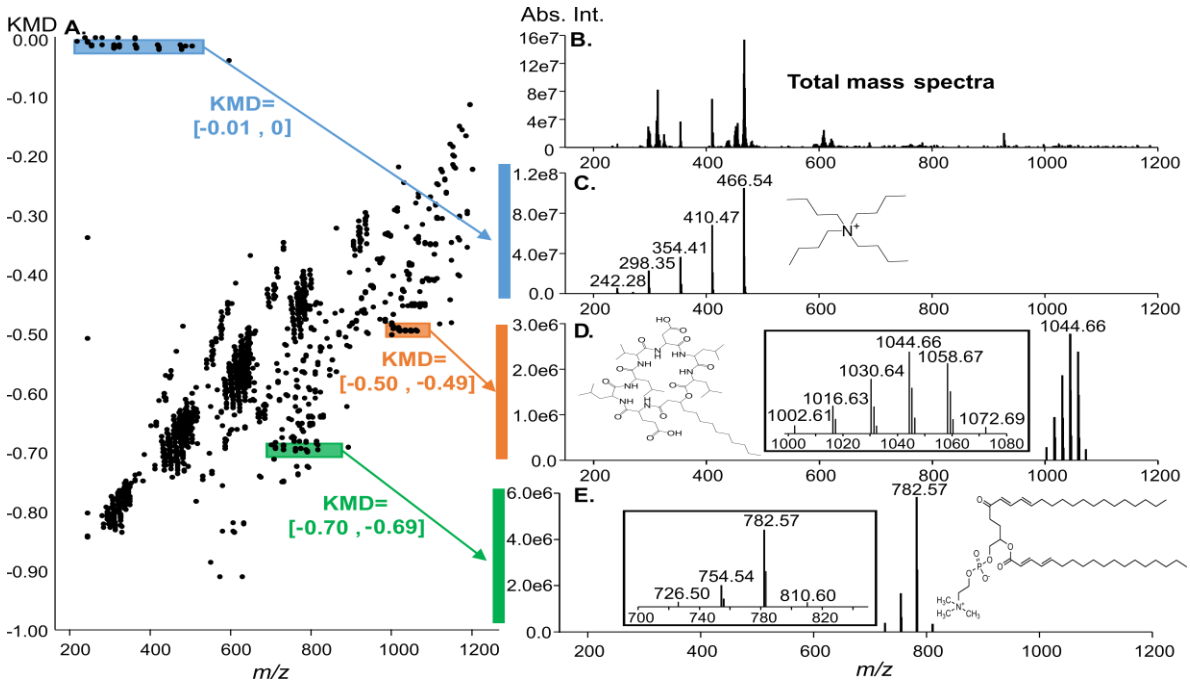

Figure 2: Illustration of the KMD filtering method. (A) Kendrick mass defect plot of the spectra obtained by FT-ICR MS. (B) Full MS spectra when no filtration is applied. By selecting a specific KMD range and eventually a specific mass range, it is possible to filter the MS Spectra and show only the chemically related molecules such as TAA (C), Lipopeptides : surfactins (D) or lipids : phosphatidylcholines (E).

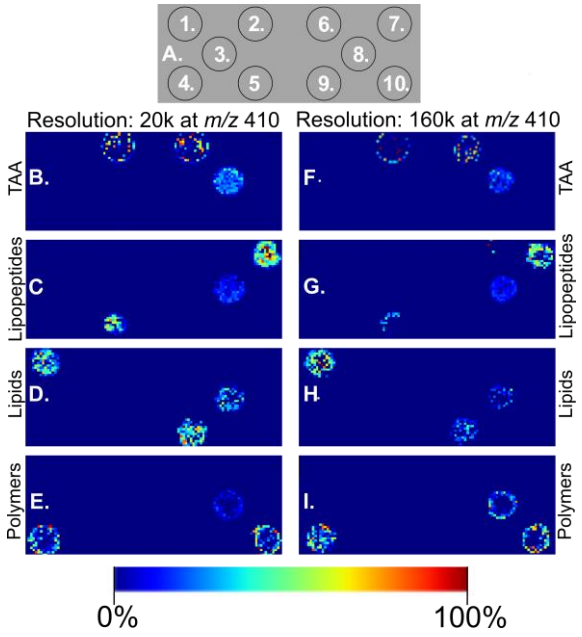

Figure 3: KMD filtering applied on MALDI mass spectrometry imaging data where different chemically-related compound were randomly spotted on a MALDI AnchorChip target plate. A. Scheme of the repartition of chemically-related compounds (Spots 1. and 9.: Lipids, spots 2. and 6.: Tetraalkylammonium, spot 3.: Matrix, spot 4. and 10.: Polymers, spots 5. and 7.: Lipopeptides, spot 8.: Mix). B to E are generated image after KMD filtering for, respectively, TAA, lipopeptides, lipids and polymers from MSI data with a MS resolution of FWHM 20,000 for *m/z* 410. F to I are generated image after KMD filtering for, respectively, TAA, lipopeptides, lipids and polymers from MSI data with a MS resolution of FWHM 160,000 for *m/z* 410. The color scale represents the normalized intensity of the ions.

MALDI Imaging of bacterial culture. Mass spectrometry imaging of culture of bacteria and more precisely the molecular imaging of their interactions in complex samples has gained growing attention[14, 16-19]. Mass spectrometry imaging is used to identify (based on the exact masses and potentially tandem MS) the molecular origin of a visible phenomenon such as compounds responsible for growth inhibition[20]. The application of Kendrick filtering to images seems well suitable in this case. Indeed, the objective is to detect known compounds or identify new related ones, such as lipopeptides, produced by the bacteria in different environments or at different elapsed times of growing. Since most of these compounds contain a variable lipid chain length[21], using a KMD plot with a $-CH_2-$ unit enables a fast identification and localization of the compounds of interest, even when detected in low intensity. The results were analyzed according to a non-targeted approach, by screening along the KMD axis different families of compounds (Figure 4). These compounds were then identified based on their exact mass. Three different families of lipopeptides were detected, and identified as iturins (Figure 4.B), surfactins (Figure 4.C) and sessilins (Figure 4.F). As expected, the distribution of lipopeptides differs according to the different families. Surfactins and iturins are produced by *Bacillus* and excreted in the agar medium, suggesting an interplay between *Bacillus* and *Pseuomonas*[22]. On the opposite, the sessilins are accumulating in *Pseudomonas*, but are not detected outside of the bacterial colony.

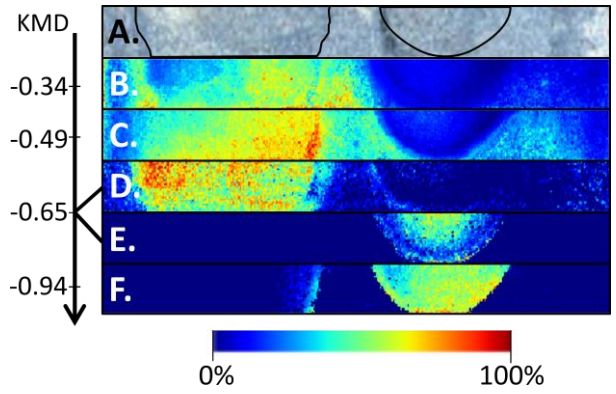

Figure 4: KMD filtering applied on MALDI Imaging of bacterial culture. (A) optical image of the sample covered with matrix, *Pseudomonas* is circled at the left side, and *Bacillus* is circled at the right side. The identified families are presented according to their KMD value. (B) Iturins A (sodium adducts) at the KMD range -0.33 to -0.35 (C) Surfactins (sodium adducts) at the KMD range -0.49 to -0.51. (D) and (E) identification of two different lipid classes at the KMD range -0.65 to -0.66, (F) Sessilins (sodium adducts) at the KMD range -0.93 to -0.95. The color scale represents the normalized intensity of the ions.

In the KMD range -0.65 to -0.66, at least two different lipid families were detected (Figure 4, D and E). Thanks to the mass difference clustering algorithm, it is possible to separate these two groups. The first group of lipids (Figure 4.D) contained the *m/z* values: 710.444, 724.459 and 738.477, belonging to the sub class 1-(1Z-alkenyl)2-acylglycerophosphoethanolamines of the glycerophosphoethanolamines lipid class. Based on their localization on the ITO slide, this lipid group was specific to Bacillus velezensis S499. The second group of lipids (Figure 4.E) composed of the *m/z* values; 734.472 and 748.487 was identified as diacylglycerophosphoethanolamines or diacylglycerophosphocholines. Their spatial distribution was specific to *Pseudomonas sp. CMR12a*.

MALDI imaging of a mouse brain section. The application of MSI imaging on mice enables to localize a set of diverse molecules in a specific tissue, such as brain[23], liver[24] or kidney[25], providing local molecular information for a better understating of illnesses of physiological mechanism. Among the detected compounds, lipids represent a high percentage of ions since they are present in every cell by constituting the membranes and energy storage vesicles[26, 27]. Their implication in various biological functions and their capacity to reflect the physiological and environmental conditions makes their study essential for disease understanding or biomarker discovery[28-31]. The results obtained by MSI of a mouse brain tissue (Figure 5) shows different patterns of lipid distribution belonging to the glycerophosphocholines (GPCs), the glycerophosphoacids (GPAs), the Glycerophosophoenthanolamines (GPEs) and the hexosylceramides (HexCers) class.

Furthermore, given that the presence of unsaturation within the lipid chain will affect its KMD value (integer value shifts only), using the KMD filtering allows to easily reconstruct images of lipids based on their unsaturation level.

Interestingly, after our Kendrick filtering strategy, some of the detected lipids on the brain tissue sections from mouse were easily observed to be differentially co-localized. The degree of unsaturation located on the lipids having double alkyl chains seems to induce a different distribution for both GPA and GPC. When the GPAs and GPCs are fully saturated, lipids are located mainly in the cerebral cortex and the cerebellar cortex (Figure 5, A and D respectively). At more than two unsaturation's, GPAs are mostly located in the fiber tracks (Figure 5 B and C respectively). One should note that GPCs with four unsaturation's were not found in the cerebellum nor the fiber tracks, but only in the hippocampal formation and cerebral nuclei (F). Finally, some other interesting lipid repartitions can also be detected, such as the specific localization of HexCers in the fiber tracts (G) or the localization of GPEs in the cerebral cortex (H).

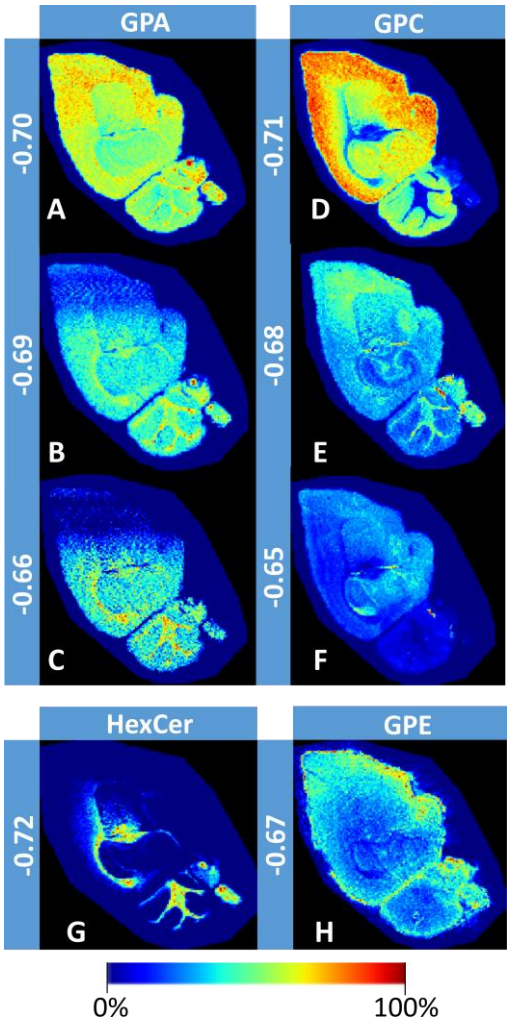

Figure 5. KMD filtering applied on MALDI imaging of a mouse brain. (A) – (C) corresponds to different dicaylglycerophosphates (GPA) with either 0, 2 or 4 unsaturation's. (D)-(F) corresponds to glycerophosphocholines (GPC) at 0, 2 or 4 unsaturation's. (G) represents the HexCer group and (H) represents the glycerophosophoenthanolamines (GPE) with one unsaturation. The color scale represents the normalized intensity of the ions.

With this KMD MSI data filtering, any type of biological modification occurring on lipids such as shorter or longer lipid chain length or lipid oxidation could be easily detected on the KMD plot. Image reconstruction based on the KMD plot provides, for a given KMD range, a specific lipid fingerprint that can further be used to compare different images.

CONCLUSION

In this work, we have used the KMD as a filtering tool to visualize the chemically related compounds in complex mass spectra, as described in the literature. The resolution and mass

accuracy of modern instruments allows a precise KMD filtering. For overlapping families, a second filtering using the mass distance between peaks has been introduced. Based on those selection criteria, we were able to group compounds presenting the same KMD in a single spectrum and to apply the KMD analysis to molecular images obtained by MALDI MSI where it reveals all its power. Replacing the *m/z* axis of the reconstructed mean mass spectrum by a KMD axis brings a real benefit for rapid and automatic image reconstruction not only for specific organic molecules but also for families, speeding up the identification process and facilitating data analysis. The developed approach has been successfully applied through two practical examples, e.g. bacterial culture and histological section of mouse brain. KMD filtering method applied to bacterial culture image data has allowed the rapid detection and localization of different groups of compounds, such as lipopeptides or lipids. The application of KMD filtering method to histological sections of a mouse brain, has allowed us to localize lipids in function of their family and their number of unsaturation.

In light of these results, we argue that the methodology outlined in this paper can be used as a non-targeted screening tool, reconstructing the image by scanning the KMD scale according to the workflow proposed in Figure 1. Non-targeted, semi targeted or targeted mode are different options developed in the software, allowing to rapidly detect and localize metabolites containing the repetitive unit of the substrate molecule or a specific family of compounds, through their known KMD. The same approach is can be extended to any type of data sets in mass spectrometry imaging with different ionization process (e.g., MALDI, DESI, SIMS MSI) but also when MS is hyphenated with separation methods, no matter the separation method employed (e.g., ion mobility or liquid chromatography) nor the mass analyzers used.

AUTHOR INFORMATION

Corresponding Author

*E-mail : e.depauw@uliege.be.

Author Contributions

‡These authors contributed equally.

Notes

The authors declare no competing financial interest.

ACKNOWLEDGMENT

The authors want to thank Prof. Philippe Jacques, from the Microbial Processes and Interactions (MiPI) research unit of Gembloux Agro-Bio Tech (Belgium) and Lipofabrik (Lille, France) for providing lipopeptides samples.

The authors acknowledge financial support from the Excellence Of Science Program of the FNRS F.R.S (Rhizoclip EOS2018000802), from the Interreg EMR project: EURLIPIDS (R-8598) and from the European Union's Horizon 2020 research and innovation program under grant agreement No. 731077.

All experiments were done with permission from the Committee on Animal Welfare of Maastricht University, according to Dutch governmental rules.

REFERENCES

1. Schmitt-Kopplin, P.; Hertkorn, N., Ultrahigh resolution mass spectrometry. *Analytical and Bioanalytical Chemistry* **2007,** *389* (5), 1309-1310.
2. Cho, Y.; Ahmed, A.; Islam, A.; Kim, S., Developments in FT-ICR MS instrumentation, ionization techniques, and data interpretation methods for petroleomics. *Mass spectrometry reviews* **2015,** *34* (2), 248-263.
3. Kendrick, E., A Mass Scale Based on CH2 = 14.0000 for High Resolution Mass Spectrometry of Organic Compounds. *Analytical Chemistry* **1963,** *35* (13), 2146-2154.
4. Roach, P. J.; Laskin, J.; Laskin, A., Higher-Order Mass Defect Analysis for Mass Spectra of Complex Organic Mixtures. *Analytical Chemistry* **2011,** *83* (12), 4924-4929.
5. Hughey, C. A.; Hendrickson, C. L.; Rodgers, R. P.; Marshall, A. G.; Qian, K., Kendrick Mass Defect Spectrum: A Compact Visual Analysis for Ultrahigh-Resolution Broadband Mass Spectra. *Analytical Chemistry* **2001,** *73* (19), 4676-4681.
6. Marshall, A. G.; Rodgers, R. P., Petroleomics: The Next Grand Challenge for Chemical Analysis. *Accounts of Chemical Research* **2004,** *37* (1), 53-59.
7. Morgan, T. E.; Ellacott, S. H.; Wootton, C. A.; Barrow, M. P.; Bristow, A. W. T.; Perrier, S.; O'Connor, P. B., Coupling Electron Capture Dissociation and the Modified Kendrick Mass Defect for Sequencing of a Poly(2-ethyl-2-oxazoline) Polymer. *Analytical Chemistry* **2018,** *90* (19), 11710-11715.
8. Lerno, L. A.; German, J. B.; Lebrilla, C. B., Method for the Identification of Lipid Classes Based on Referenced Kendrick Mass Analysis. *Analytical Chemistry* **2010,** *82* (10), 4236-4245.
9. Nakamura, S.; Cody, R. B.; Sato, H.; Fouquet, T., Graphical Ranking of Divisors to Get the Most out of a Resolution-Enhanced Kendrick Mass Defect Plot. *Analytical Chemistry* **2019,** *91* (3), 2004-2012.
10. Zheng, Q.; Morimoto, M.; Sato, H.; Fouquet, T., Resolution-enhanced Kendrick mass defect plots for the data processing of mass spectra from wood and coal hydrothermal extracts. *Fuel* **2019,** *235*, 944-953.
11. Roullier-Gall, C.; Witting, M.; Gougeon, R. D.; Schmitt-Kopplin, P., High precision mass measurements for wine metabolomics. *Frontiers in Chemistry* **2014,** *2* (102).
12. Matyash, V.; Liebisch, G.; Kurzchalia, T. V.; Shevchenko, A.; Schwudke, D., Lipid extraction by methyl-tert-butyl ether for high-throughput lipidomics. *Journal of lipid research* **2008,** *49* (5), 1137-46.
13. Youmans, K. L.; Tai, L. M.; Nwabuisi-Heath, E.; Jungbauer, L.; Kanekiyo, T.; Gan, M.; Kim, J.; Eimer, W. A.; Estus, S.; Rebeck, G. W.; Weeber, E. J.; Bu, G.; Yu, C.; Ladu, M. J., APOE4-specific changes in Abeta accumulation in a new transgenic mouse model of Alzheimer disease. *The Journal of biological chemistry* **2012,** *287* (50), 41774-86.
14. Debois, D.; Ongena, M.; Cawoy, H.; De Pauw, E., MALDI-FTICR MS imaging as a powerful tool to identify Paenibacillus antibiotics involved in the inhibition of plant pathogens. *J Am Soc Mass Spectrom* **2013,** *24* (8), 1202-13.
15. Chambers, M. C.; Maclean, B.; Burke, R.; Amodei, D.; Ruderman, D. L.; Neumann, S.; Gatto, L.; Fischer, B.; Pratt, B.; Egertson, J.; Hoff, K.; Kessner, D.; Tasman, N.; Shulman, N.; Frewen, B.; Baker, T. A.; Brusniak, M. Y.; Paulse, C.; Creasy, D.; Flashner, L.; Kani, K.; Moulding, C.; Seymour, S. L.; Nuwaysir, L. M.; Lefebvre, B.; Kuhlmann, F.; Roark, J.; Rainer, P.; Detlev, S.; Hemenway, T.; Huhmer, A.; Langridge, J.; Connolly, B.; Chadick, T.; Holly, K.; Eckels, J.; Deutsch, E. W.; Moritz, R. L.; Katz, J. E.; Agus, D. B.; MacCoss, M.; Tabb, D. L.; Mallick, P., A cross-platform toolkit for mass spectrometry and proteomics. *Nat Biotechnol* **2012,** *30* (10), 918-20.
16. Yang, J. Y.; Phelan, V. V.; Simkovsky, R.; Watrous, J. D.; Trial, R. M.; Fleming, T. C.; Wenter, R.; Moore, B. S.; Golden, S. S.; Pogliano, K.; Dorrestein, P. C., Primer on Agar-Based Microbial Imaging Mass Spectrometry. *Journal of Bacteriology* **2012,** *194* (22), 6023-6028.
17. Debois, D.; Jourdan, E.; Smargiasso, N.; Thonart, P.; De Pauw, E.; Ongena, M., Spatiotemporal Monitoring of the Antibiome Secreted by Bacillus Biofilms on Plant Roots Using MALDI Mass Spectrometry Imaging. *Analytical Chemistry* **2014,** *86* (9), 4431-4438.
18. Boya P, C. A.; Fernández-Marín, H.; Mejía, L. C.; Spadafora, C.; Dorrestein, P. C.; Gutiérrez, M., Imaging mass spectrometry and MS/MS molecular networking reveals chemical

interactions among cuticular bacteria and pathogenic fungi associated with fungus-growing ants. *Scientific Reports* **2017,** *7* (1), 5604.

19. Dunham, S. J. B.; Ellis, J. F.; Li, B.; Sweedler, J. V., Mass Spectrometry Imaging of Complex Microbial Communities. *Accounts of Chemical Research* **2017,** *50* (1), 96-104.

20. Gonzalez, D. J.; Haste, N. M.; Hollands, A.; Fleming, T. C.; Hamby, M.; Pogliano, K.; Nizet, V.; Dorrestein, P. C., Microbial competition between Bacillus subtilis and Staphylococcus aureus monitored by imaging mass spectrometry. *Microbiology (Reading, England)* **2011,** *157* (Pt 9), 2485-92.

21. Ongena, M.; Jacques, P., Bacillus lipopeptides: versatile weapons for plant disease biocontrol. *Trends Microbiol* **2008,** *16*.

22. Molina-Santiago, C.; Pearson, J. R.; Navarro, Y.; Berlanga-Clavero, M. V.; Caraballo-Rodriguez, A. M.; Petras, D.; Garcia-Martin, M. L.; Lamon, G.; Haberstein, B.; Cazorla, F. M.; de Vicente, A.; Loquet, A.; Dorrestein, P. C.; Romero, D., The extracellular matrix protects Bacillus subtilis colonies from Pseudomonas invasion and modulates plant co-colonization. *Nature communications* **2019,** *10* (1), 1919.

23. Stoeckli, M.; Staab, D.; Staufenbiel, M.; Wiederhold, K.-H.; Signor, L., Molecular imaging of amyloid β peptides in mouse brain sections using mass spectrometry. *Analytical Biochemistry* **2002,** *311* (1), 33-39.

24. Shimma, S.; Sugiura, Y.; Hayasaka, T.; Hoshikawa, Y.; Noda, T.; Setou, M., MALDI-based imaging mass spectrometry revealed abnormal distribution of phospholipids in colon cancer liver metastasis. *Journal of Chromatography B* **2007,** *855* (1), 98-103.

25. Zoriy, M.; Matusch, A.; Spruss, T.; Becker, J. S., Laser ablation inductively coupled plasma mass spectrometry for imaging of copper, zinc, and platinum in thin sections of a kidney from a mouse treated with cis-platin. *International Journal of Mass Spectrometry* **2007,** *260* (2), 102-106.

26. Murphy, R. C.; Hankin, J. A.; Barkley, R. M., Imaging of lipid species by MALDI mass spectrometry. *Journal of lipid research* **2009,** *50 Suppl*, S317-22.

27. Burnum, K. E.; Cornett, D. S.; Puolitaival, S. M.; Milne, S. B.; Myers, D. S.; Tranguch, S.; Brown, H. A.; Dey, S. K.; Caprioli, R. M., Spatial and temporal alterations of phospholipids determined by mass spectrometry during mouse embryo implantation. *Journal of lipid research* **2009,** *50* (11), 2290-2298.

28. Wenk, M. R., The emerging field of lipidomics. *Nature Reviews Drug Discovery* **2005,** *4* (7), 594-610.

29. Orešič, M.; Hänninen, V. A.; Vidal-Puig, A., Lipidomics: a new window to biomedical frontiers. *Trends in Biotechnology* **2008,** *26* (12), 647-652.

30. Yang, K.; Han, X., Lipidomics: Techniques, Applications, and Outcomes Related to Biomedical Sciences. *Trends in Biochemical Sciences* **2016,** *41* (11), 954-969.

31. Lam, S. M.; Shui, G., Lipidomics as a Principal Tool for Advancing Biomedical Research. *Journal of Genetics and Genomics* **2013,** *40* (8), 375-390.

Supporting information

Rapid visualization of chemically related compounds using Kendrick mass defect as a filter in mass spectrometry imaging

Kune Christopher[a]‡ and Mc Cann Andréa[a]‡, La Rocca Raphaël[a], Arguelles Arias Anthony[b], Tiquet Mathieu[a], Van Kruining Daan[c], Martinez Martinez Pilar[c], Ongena Marc[b], Eppe Gauthier[a], Quinton Loïc[a], Far Johann[a], De Pauw Edwin[a*]

‡These authors contributed equally

Full detailed experimental section:

Human Glu-1-Fibrinopeptide B (Glu-Fib) and Bovine Serum Albumin (BSA) were purchased from Sigma-Aldrich (Belgium). Glu-Fib was dissolved in water with 10 % of acetonitrile and 0.1 % of formic acid to obtain a stock solution of 250 µM and kept at -20 °C until use. BSA was dissolved in a buffering solution of 50mM ammonium bicarbonate at pH 8. Disulfide bonds were reduced using dithiothreitol and stabilized with iodoacetamide. BSA was then digested with Trypsin (Pierce trypsin protease, MS grade from Thermo scientific) in a protein to enzyme ratio of 1/100 at 37 °C overnight. The resulting solution was dried by speed vacuum and stored at -20 °C until use. The Glu-Fib or trypsin digested BSA was dissolved in a 50 % methanol solution with 0.1 % formic acid at a final concentration of 15 µM for mass spectrometry infusion using 250 µL Hamilton syringe at 4 µL/min.

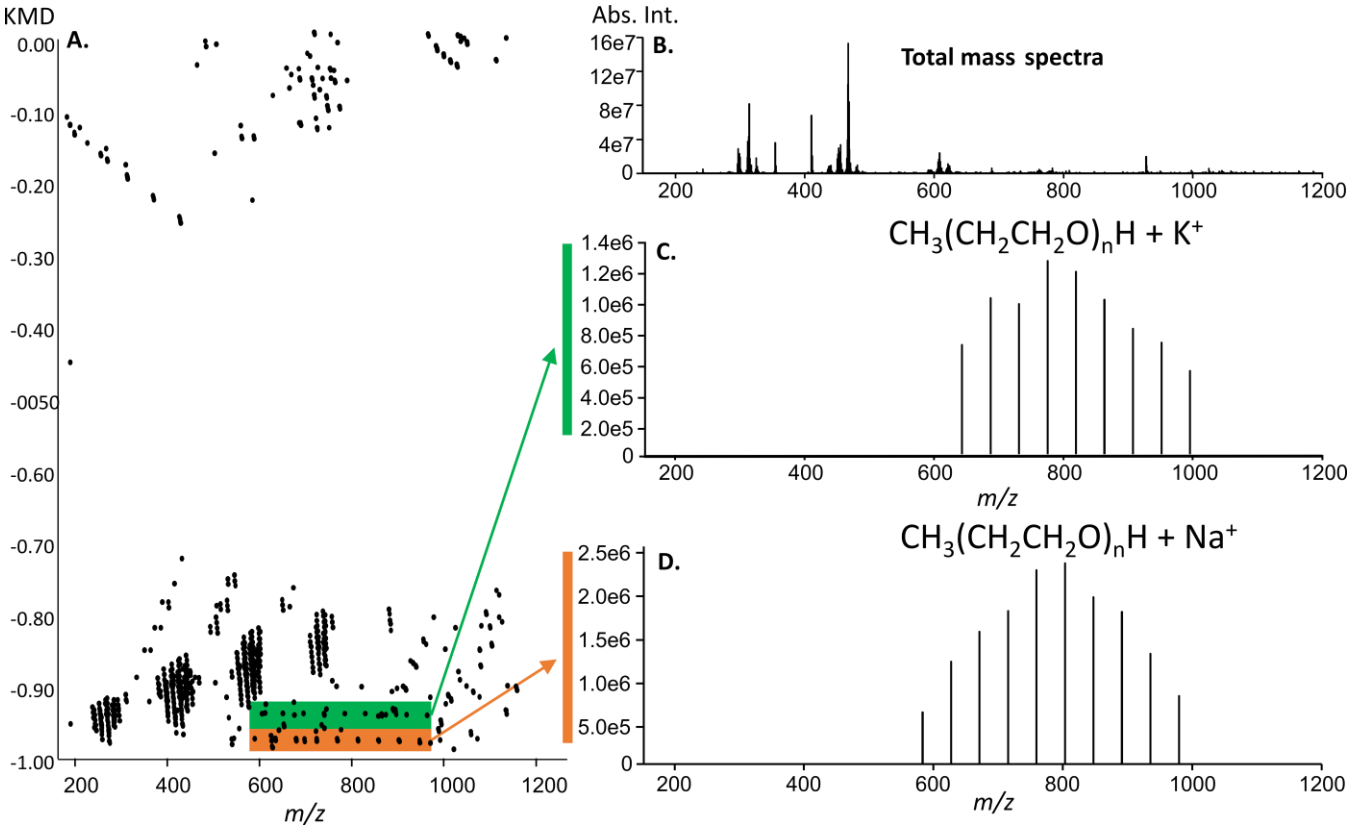

Figure S2: KMD analysis applied on polymers: